

Thermal structures and heat transfer in wall-bounded flows at transcritical conditions

By J. Guo, X. I. A. Yang[†] AND M. Ihme

1. Motivation and objectives

Transcritical flows are observed for fluids at high pressures crossing the Widom line, which is formally defined as the line emanating from the critical point where the specific heat capacity is maximum at a given pressure (Simeoni *et al.* 2010). Fluid properties vary considerably in this regime, as the fluid transforms from a liquid-like fluid to a vapor-like fluid. For observed fluids in transcritical conditions, there is typically a sharp decrease in magnitude of properties such as density, speed of sound, and viscosity (Yoo 2013). However, this transition is accompanied by a rapid increase in specific heat, which also corresponds with a noticeable change in turbulent heat transfer (Kawai 2016; Piro *et al.* 2004).

Transcritical flows, with an emphasis on flows entering into and existing in the high-pressure supercritical phase, are frequently encountered in engineering applications, including in regenerative cooling systems in liquid rocket motors, gas turbines, internal combustion engines, steam generators in power plants, and refrigeration systems. Other processes include supercritical water oxidation for waste treatment, fluid extraction, chromatography, and polymer processing (Piro *et al.* 2004).

Despite this prevalence of transcritical flows, the thermo-viscous structure of the boundary layer and associated heat transfer are only incompletely understood, leading to a general need for the development of accurate predictive models. Generally used assumptions for previously studied flows at other thermodynamic conditions do not usually yield acceptable results, partly because fluids in transcritical conditions are neither calorically perfect nor incompressible, leading to invalidity of many of the usual simplifying assumptions used in formulation and calculation of such flows (Pizzarelli *et al.* 2009). Experimental data (and related turbulence statistics) are difficult to obtain, due to the high-pressure conditions that are inherent to supercritical flows. Reynolds-averaged Navier-Stokes (RANS) models are also deficient, and it is difficult to extract meaningful results from them, owing to a lack of reliable validation data (Yoo 2013). Thus, direct numerical simulation (DNS) is the currently employed standard for transcritical flow analysis, despite the conditions of low Reynolds number and high computational cost. While there is a push toward large-eddy simulation (LES) analysis of transcritical flows as a trade-off between RANS and DNS in computational cost and accuracy, DNS is currently used as the only validated and viable tool in the analysis of turbulent statistics, turbulent structures, heat transfer/skin friction characteristics, and model validation.

The main objective of this work is to examine the DNS of transcritical wall-bounded flows, with a focus on analysis of thermal boundary layer structure. We investigate scaling relations that transform the temperature into a canonical logarithmic law of the wall, via wall units and semi-local scaling. The validity of the attached-eddy model is

[†] Mechanical and Nuclear Engineering Department, Pennsylvania State University

also investigated. The results of this analysis are proposed as a means to inform future high-fidelity computational fluid dynamics models, especially in the development of wall-modeled LES. The remainder of this report is organized as follows. A detailed overview of existing theory for the law of the wall and a novel temperature transformation are presented in Section 2. The computational setup and DNS aspects are discussed in Section 3. Results for mean flow, instantaneous flow field, thermal energy spectra, and second-order statistics are discussed in Section 4. Finally, concluding remarks and suggested paths forward are offered in Section 5.

2. Formulation

Through a self-similar solution method of the near-wall simplified boundary layer equations, constant-property wall-bounded flows follow the velocity law of the wall. The velocity boundary layer for wall unit-normalized streamwise velocity u^+ and wall-normal distance y^+ (Pope 2001) is formulated as

$$\overline{u^+} = \begin{cases} y^+ & \text{viscous sublayer, } y^+ < 5 \\ \frac{1}{\kappa} \log(y^+) + B & \text{logarithmic region, } 30 \lesssim y^+ \lesssim 0.1\delta \end{cases}, \quad (2.1)$$

where κ is the von Kármán constant with $\kappa \approx 0.4$ and B is a constant with $B \approx 5$. The $+$ superscript indicates wall units, which are normalized by the wall-evaluated friction velocity and length scale $u_\tau = \sqrt{\tau_w/\rho_w}$ and $\delta_\nu = \mu_w/(\rho_w u_\tau)$, respectively. The wall-normal distance and streamwise velocity are $y^+ = y/\delta_\nu$ and $\overline{u^+} = \overline{u}/u_\tau$, respectively.

The subscript w indicates values of quantities evaluated at the wall. Here, the single overline ($\overline{\quad}$) denotes Reynolds averaging. A key objective of this report is to analyze the law of the wall for time-averaged mean temperature $\overline{\theta}$, which is defined as

$$\overline{\theta} = \overline{T} - T_w, \quad (2.2)$$

where T_w is the temperature at the wall.

2.1. Temperature law-of-the-wall analogy

Several attempts to explain the temperature collapse have been proposed that follow the same form as the classical law of the wall. Notably, Kader (1981) proposed the following relation

$$\overline{\theta^+} = \begin{cases} Pr y^+ & \text{viscous sublayer, } y^+ < 5 \\ 2.12 \ln(y^+) + \beta(Pr) & \text{logarithmic region, } 30 \lesssim y^+ \lesssim 0.1\delta \end{cases}, \quad (2.3)$$

where the molecular Prandtl number (given as the ratio of momentum diffusivity to thermal diffusivity) is

$$Pr = \frac{\nu}{\alpha} \quad (2.4)$$

and β is given by the logarithmic region algebraic expression $\beta(Pr) = (3.85Pr^{1/3} - 1.3)^2 + 2.12 \ln Pr$. In the results for wall scaling, we have used the Prandtl number at the wall, i.e., $Pr = Pr_w$. The specific formulation of this log-law involves an assumption of dominant molecular heat transfer near the wall, and general similarity arguments for matching with experimental data in the log layer. Note that this law of the wall uses several assumptions:

(a) Heat is a passive scalar. While this assumption does not hold true for transcritical flows, meaningful insight can still be obtained from this formulation, notably the Prandtl number dependence.

(b) The turbulent Prandtl number Pr_t is independent of Pr , meaning that eddy viscosity and eddy thermal diffusion are determined by velocity and temperature fluctuations only.

This formulation will be used for comparison in Section 4. Although these approximations and conditions used do not quite satisfy those of the current wall-bounded transcritical flow that this paper is analyzing, the formulation can still provide meaningful insight, especially when serving as a means of comparison.

Compressible flows must be considered in terms of fluid properties that are functions of temperature and pressure. These variations in physical properties introduce strong deviations from classical law of the wall formulations. Transcritical flows exhibit strong variability in density, viscosity, heat capacity, and other properties. A consequence is that the time-averaged velocity and temperature do not follow a law of a wall relation without a scaling transformation. A commonly used transformation for collapsing the velocity with the wall-normal distance y^+ is the van Driest transformation (van Driest 1951)

$$\overline{u_{VD}^+} = \int_0^{\overline{u^+}} \left[\frac{\overline{\rho}}{\overline{\rho_w}} \right]^{1/2} d\overline{u^+}. \quad (2.5)$$

$\overline{\theta^+}$ is normalized by

$$T_\tau = \theta_\tau = \frac{q_w}{\rho_w c_{p,w} u_\tau}, \quad (2.6)$$

such that the normalized temperature is $\overline{\theta^+} = \overline{\theta}/\theta_\tau$. The analogous temperature transformation that follows this van Driest form is

$$\overline{\theta_{VD}^+} = \int_0^{\overline{\theta^+}} \left[\frac{\overline{\rho c_p}}{\overline{\rho_w c_{p,w}}} \right]^{1/2} d\overline{\theta^+}. \quad (2.7)$$

By assuming independence between ρ and c_p (which is equivalent to making the assumption that $\overline{\rho c_p} \simeq \overline{\rho} \overline{c_p}$), this expression can also be simplified to

$$\overline{\theta_{VD}^+} \simeq \int_0^{\overline{\theta^+}} \left[\frac{\overline{\rho} \overline{c_p}}{\overline{\rho_w} \overline{c_{p,w}}} \right]^{1/2} d\overline{\theta^+}. \quad (2.8)$$

The resulting implications of this simplification on the temperature profile are discussed later, in Section 4.

These van Driest-transformed functions are expected to collapse with y^+ , with a linear dependency on the local Prandtl number (Kader 1981).

2.2. Trettel-Larsson-like transformation

Boundary profiles with nonadiabatic walls exhibit deficiencies in collapsing the velocity to a log-law without a transformation. While the van Driest-transformed velocity u_{VD}^+ was found to collapse to the classical law of the wall for boundary layer flows with adiabatic wall conditions (Ma *et al.* 2018), the case of non-adiabatic walls requires a different transformation, such as that derived by equating the turbulent momentum flux and the viscous stress to their respective incompressible counterparts (Trettel & Larsson 2016). In this approach, Trettel and Larsson developed a transformation considering the dominant

effects of compressibility on the mean property variation of density and viscosity to derive a universality of the inner layer profiles for wall-bounded turbulent flows, resulting in

$$y_{SL} = \frac{y\sqrt{\tau_w \bar{\rho}}}{\bar{\mu}} \quad (2.9)$$

and

$$\overline{u_{TL}^+} = \int_0^{\overline{u^+}} \left(\frac{\bar{\rho}}{\bar{\rho}_w} \right)^{1/2} \left[1 + \frac{1}{2} \frac{1}{\bar{\rho}} \frac{d\bar{\rho}}{dy} y - \frac{1}{\bar{\mu}} \frac{d\bar{\mu}}{dy} y \right] d\overline{u^+}. \quad (2.10)$$

Following this transformation, $\overline{u_{TL}^+}$ is expected to collapse to the law of the wall as a function of y_{SL} . The subscript SL denotes a semi-local scaling, and the subscript TL refers to the formulation done by Trettel & Larsson (2016). Further discussion is provided by Ma *et al.* (2018).

Following the derivation done by Trettel & Larsson (2016), we proceed by considering the following three-part approach:

- (a) derivation of a log-law condition,
- (b) derivation of a stress balance condition, and
- (c) combination of the two to obtain a full transformation.

The goal is to derive a self-similar solution of the compressible fluid boundary layer temperature field. The compressible state is characterized by mean scaled temperature $\bar{\theta}$, density $\bar{\rho}$, constant-pressure specific heat capacity \bar{c}_p , and viscosity $\bar{\mu}$. The incompressible, transformed state has constant values of density, viscosity, and specific heat ρ_w , μ_w , and $c_{p,w}$, respectively, as well as mean scaled temperature $\bar{\Theta}$. By definition, the two states share the same wall heat flux q_w , which is analogous to wall shear stress τ_w in the velocity transformation by Trettel & Larsson (2016). The two states share the same friction temperature, defined as

$$\theta_\tau = \frac{q_w}{\rho_w c_{p,w} u_\tau}, \quad (2.11)$$

and the same viscous length scale as before,

$$l_\nu = \frac{\mu_w}{\rho_w u_\tau}, \quad (2.12)$$

for the friction velocity u_τ , as defined previously.

As also outlined by Trettel & Larsson (2016), because the two states share the same scaling, the transformation from physical values to universal quantities implies $y \rightarrow Y^+$ and $\bar{\theta} \rightarrow \bar{\Theta}^+$. The proposed transformation is expanded using the chain rule as

$$\frac{d\bar{\Theta}}{dY} = \frac{d\bar{\Theta}}{d\bar{\theta}} \frac{d\bar{\theta}}{dY} \frac{dY}{dy}. \quad (2.13)$$

The resultant transformations are given by

$$\bar{\Theta} = \int_0^{\bar{\theta}^+} \frac{d\bar{\Theta}}{d\bar{\theta}} d\bar{\theta}^+ \quad (2.14)$$

and

$$Y = \int_0^{y^+} \frac{dY}{dy} dy^+. \quad (2.15)$$

2.2.1. Log-law condition

We assume that the temperature gradient in the log-layer is not affected by diffusive effects, which is an analogy to the independence of the velocity log-layer with respect to diffusive effects (Schlichting & Gersten 2000). Dimensional analysis then leads us to define the temperature gradients

$$\frac{d\bar{\theta}}{dy} = \frac{1}{\kappa^*} \frac{1}{y} \frac{q_w}{\rho c_p u_\tau} \simeq \frac{1}{\kappa^*} \frac{1}{y} \frac{q_w}{\sqrt{\tau_w \rho c_p^2}} \quad (2.16)$$

and

$$\frac{d\bar{\Theta}}{dY} = \frac{1}{\kappa^*} \frac{1}{Y} \frac{q_w}{\rho_w c_{p,w} u_\tau} = \frac{1}{\kappa^*} \frac{1}{Y} \frac{q_w}{\sqrt{\tau_w \rho_w c_{p,w}^2}} \quad (2.17)$$

for a constant log-law factor κ^* , analogous to the velocity law-of-the-wall von Kármán constant. Note that in writing this expression we have employed the simplification shown in Equation (2.8), such that the averaging scheme for the density and specific heat does not have a large effect on the resultant expression.

After algebraic manipulation of the above relations, we can rewrite the transformation differential for the mean temperature ($d\bar{\Theta}/d\bar{\theta}$) as

$$\frac{d\bar{\Theta}}{d\bar{\theta}} = \frac{y}{Y} \left(\frac{\bar{\rho} c_p^2}{\rho_w c_{p,w}^2} \right)^{1/2} \frac{dY}{dy}. \quad (2.18)$$

2.2.2. Stress-balance condition

As implied by Trettel & Larsson (2016), there is a connection between the temperature gradients and the heat flux, leading to the balance equation

$$-v' \rho E' + \bar{k} \frac{\partial \bar{\theta}}{\partial y} = 0 \quad (2.19)$$

for wall-normal velocity v , total energy E , and conductivity k . Assuming the temperature gradient term ($k \partial \theta / \partial y$) to be dominant, and equating the expression for the raw and transformed cases, leads to

$$k_w \frac{\partial \bar{\Theta}}{\partial Y} = \bar{k} \frac{\partial \bar{\theta}}{\partial y}, \quad (2.20)$$

which then simplifies to

$$\frac{d\bar{\Theta}}{d\bar{\theta}} = \frac{\bar{k}}{k_w} \frac{dY}{dy}. \quad (2.21)$$

Equating the expressions from the transformed temperature and stress-balance conditions leads to

$$\bar{\theta}_{TL}^+ = \int_0^{\theta^+} \sqrt{\frac{\rho c_p^2}{\rho_w c_{p,w}^2}} \left[1 + \frac{1}{2} \frac{1}{\rho c_p^2} \frac{d\rho c_p^2}{dy} y - \frac{1}{\bar{\mu}} \frac{d\bar{\mu}}{dy} y \right] d\bar{\theta}^+. \quad (2.22)$$

As in the van Driest transformation, the choice of averaging ρ and c_p would lead to two different forms of the transformation; however, the simplified/split-averaging formulation involving $\bar{\rho} \bar{c}_p^2$ is omitted here, but still plotted in the figures in Section 4.

2.3. Attached-eddy hypothesis

Following the presentation of the same theory used by Ma *et al.* (2018), the attached-eddy hypothesis is used as a model for scaling prediction of turbulent statistics in wall-bounded flows. The model consists of three hypotheses:

(a) At sufficiently high Reynolds numbers, there is a range of wall-normal distance where neither the viscous nor large-scale effects play a significant role in the turbulent statistics. This is known as the logarithmic range.

(b) The sizes of the space-filling fluid structures scale as their distance from the wall. These structures are also called attached eddies.

(c) The instantaneous velocity fluctuation at a given location is a result of the superposition of all eddy-induced velocities at that location.

The implications of the attached-eddy hypothesis for the hierarchical organization of eddies are also discussed by Ma *et al.* (2018).

3. Computational setup

The computational details, operating conditions, and DNS setup, which have largely been omitted here for brevity, are discussed in detail by Ma *et al.* (2018). Important details to note are those of the working fluid nitrogen, which is kept at a bulk reduced pressure of $p_r = p/p_c = 1.14$. The walls are confined to isothermal boundary conditions, at $T_{w,b} = 100$ K and $T_{w,t} = 300$ K, corresponding to reduced temperatures ($T_r = T/T_c$) of $T_{r,w,b} = 0.79$ and $T_{r,w,t} = 2.38$. The friction Reynolds number for the top and bottom walls is $Re_{\tau,top} = 300$ and $Re_{\tau,bottom} = 430$, respectively.

The finite-volume, fully compressible code CharLES^X, whose key details can be found in works by Khalighi *et al.* (2011) and Ma *et al.* (2017), is used for this study. The code is fourth-order accurate in space, via a central-scheme flux reconstruction on uniform meshes. The Peng-Robinson cubic equation of state is employed to close the system (Peng & Robinson 1976). Chung’s model for high-pressure fluids is employed to evaluate the molecular transport properties, including the dynamic viscosity and the thermal conductivity (Chung *et al.* 1984, 1988). The DNS grid consists of a structured grid of mesh size $N_x \times N_y \times N_z = 384 \times 256 \times 384$. A detailed grid convergence study has been performed by Ma *et al.* (2018) in order to ensure convergence of statistical flow properties.

4. Results

4.1. Mean temperature profiles

We begin with a discussion of the mean temperature profiles. Figure 1(a) shows $\overline{\theta_{VD}^+}$ as a function of y^+ , in which both the $\overline{\rho c_p}$ and $\overline{\rho c_p}$ averaging are shown. Previously, Patel *et al.* (2017) neglected the variation in c_p in computing the transformed temperature profile. Figure 1(a) includes this formulation for constant c_p for the van Driest transformation, along with the original van Driest–transformed temperatures formulated earlier in Eqs. (2.7)-(2.8). As observed, neglecting variations in c_p causes significant deviation in the mean temperature profiles from a law-of-the-wall profile, especially for wall-normal distances $y^+ > 10^2$, emphasizing the importance of c_p in this specific case of variable-property flow.

Figure 1(b) shows the same quantity (without the constant c_p approximation) as in Figure 1(a), but for the semi-local scaling with Trettel-Larsson transformation. In both

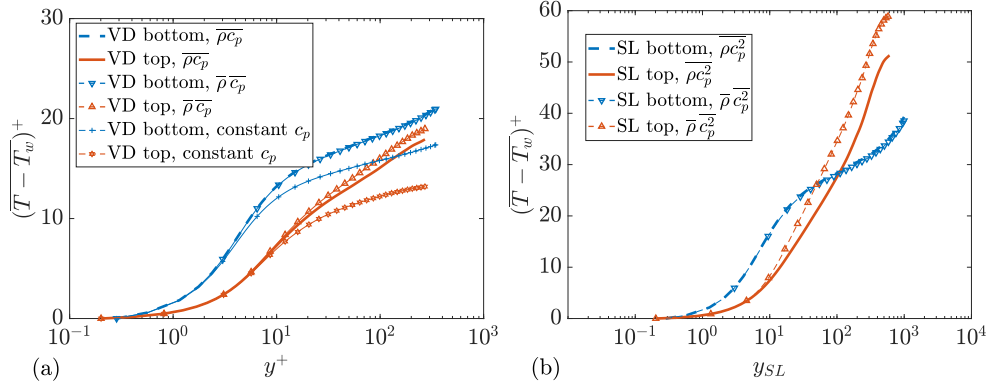


FIGURE 1. Mean temperature profiles as a function of wall-normal distance for (a) van Driest transformation, including constant c_p case, and (b) Trettel-Larsson-like transformation.

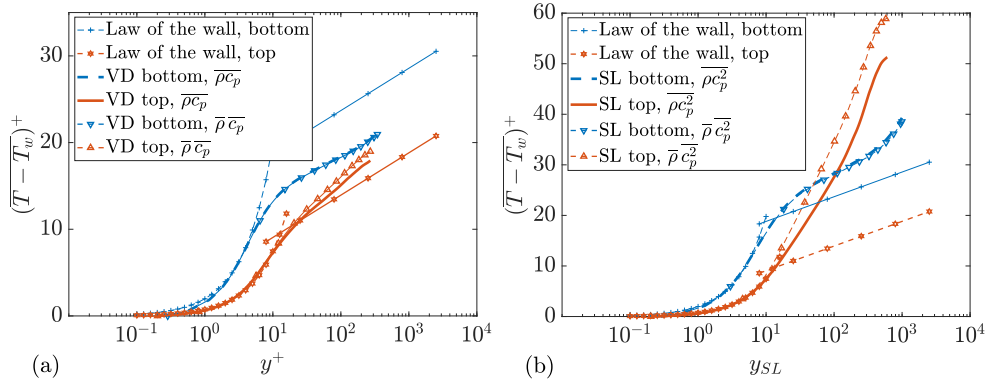


FIGURE 2. Mean temperature profiles with Kader's law-of-the-wall formulation for (a) van Driest transformation, and (b) Trettel-Larsson-like transformation.

the van Driest and the Trettel-Larsson transformations, the choice of averaging is not critical (though not negligible) to the resultant collapsed plots, except for growing deviations near the top heated wall at higher wall-normal distances.

Figures 2(a,b) shows the same van Driest and Trettel-Larsson transformations, plotted along with the law-of-the-wall formulation by Kader (1981). The log-law has been adapted such that the horizontal axis is plotted in terms of ys_L , instead of the previously formulated y^+ in Eq. (2.22). The collapse of the temperature profile (for either formulation) is not as neat as that of the mean velocity profile (Ma *et al.* 2018). In the log-layer, the van Driest transformation is more accurate for the top (heated) wall, while neither transformation is noticeably more accurate in predicting the bottom (cooled) wall. In particular, the van Driest transformation underpredicts Kader's log-law, while the semi-local scaling overpredicts it.

Note that the Trettel-Larsson transformation does very poorly near the top (heated) wall in terms of collapse. This is likely due to large gradients in c_p , which cause large variations and inaccuracies in to the c_p^2 term of the Trettel-Larsson-like derivation. Both transformations show reasonably good collapse to the linear dependency of the viscous sublayer for wall-normal distances $y^+ \lesssim 5$.

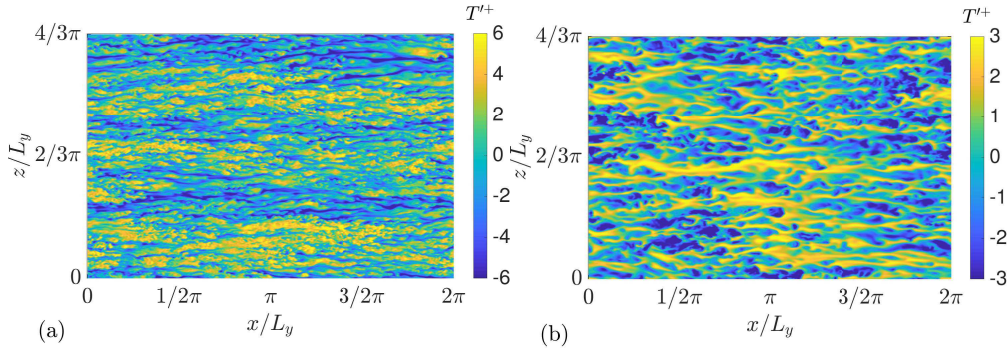


FIGURE 3. Instantaneous contours of temperature fluctuations for (a) the bottom (cooled) wall and (b) the top (heated) wall.

4.2. Instantaneous flow field, energy spectra

Figure 3 shows instantaneous contours of temperature fluctuations. Plots at larger wall normal distances (such as at $y^+ \simeq 80$, as used by Ma *et al.* (2018) for the velocity fluctuations) show few discernible structures. When the wall-normal distance is significantly decreased, observable structures become apparent. We have chosen a location in the viscous sublayer, at $y^+ = 8$, to illustrate this point.

As seen in Figure 3, the temperature fluctuation structures are qualitatively different. The high-temperature streaks in the bottom cooled wall of Figure 3(a) are localized, more densely packed, and narrower in the spanwise direction, while the streaks in the top heated wall of Figure 3(b) are less densely packed.

Similar to that observed by Sengupta *et al.* (2017), we find a higher frequency of temperature fluctuations near the bottom, cooler wall rather than at the top wall, at the same wall-normal distance. This higher frequency of fluctuations is attributed to the fact that the critical temperature of the fluid ($T_{c,N_2} = 125.2$ K) is closer to the isothermal boundary condition temperature of the bottom heated wall than that of the top heated wall. We attribute this trend to the rapid thermal property fluctuations near the critical temperature of a fluid in transcritical properties (Banuti 2015).

Figure 4 shows the thermal energy spectra as a function of the streamwise wave number, at various wall-normal distances, including the half-channel-width L_y . The reference k^{-1} slope is shown in each plot for comparison. Interestingly, while the top (heated) wall shows collapse at large scales, the bottom (cooled) wall does not display this collapsing behavior. Nevertheless, the power-law-like scaling of $\sim k^{-1}$ suggests the presence of attached eddies at both walls.

4.3. Second-order statistics

Figure 5 shows the averaged temperature fluctuation product $\overline{T'T'}$, normalized by the semi-local temperature scale and by the corresponding wall density. This is a thermal analogy to the turbulent kinetic energy. Due to the near-wall scaling of the mean flow, $\overline{T'T'}$ shows good collapse away from the wall and near the wall when y_{SL} is multiplied by the wall Prandtl number.

Figure 6 shows the correlation coefficient $R_{u\theta}$, defined as the second-order moment between temperature fluctuations and streamwise velocity fluctuations, plotted as a function of normalized wall-normal distance, for both the top and bottom walls. Specifically,

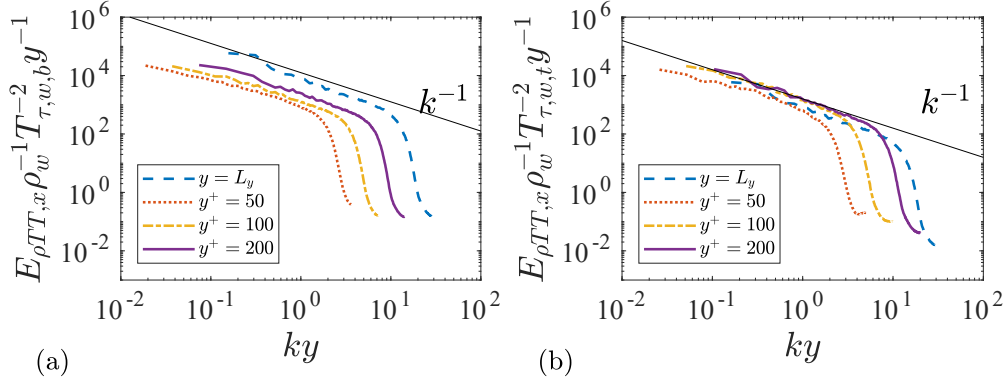


FIGURE 4. Normalized thermal energy spectra for (a) the bottom (cooled) wall and (b) the top (heated) wall.

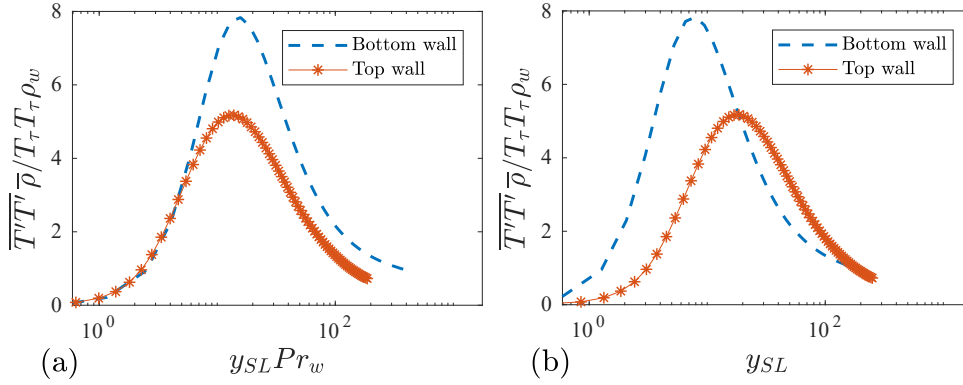


FIGURE 5. Normalized averaged temperature fluctuation product $\overline{T'T'}$, plotted against (a) $y_{SL} Pr_w$ and (b) y_{SL} .

$R_{u\theta}$ is given by

$$R_{u\theta} = \frac{\overline{u\theta}}{\sqrt{\overline{u^2} \overline{\theta^2}}}. \quad (4.1)$$

For comparison, we also include results by previous investigations from Kim & Moin (1989), Subramanian & Antonia (1981), and Yang & Abkar (2018). The dataset of Kim & Moin (1989) has friction Reynolds number $Re_{\tau} = 180$, and the experimental data from Subramanian & Antonia (1981) have Re_{τ} at various values listed below. The hierarchical random additive process model corresponds to the asymptotic prediction given and discussed by Yang & Abkar (2018).

Despite the fact that the reference results are taken from studies whose working fluids are nontranscritical (and also use domains that have identical top and bottom wall boundary conditions, as opposed to our isothermal cooled or heated walls), the results agree reasonably well with both the experimental and numerical studies for wall-normal distances approaching the wall, in magnitude of correlation. In particular, note the similarity in trend between the data from Kim & Moin (1989) and both our cooled and heated walls, most notably the peak at $y^+ \simeq 10$. Interestingly, despite the complications introduced by the presence of real fluids and transcritical conditions, this $R_{u\theta}$ correlation

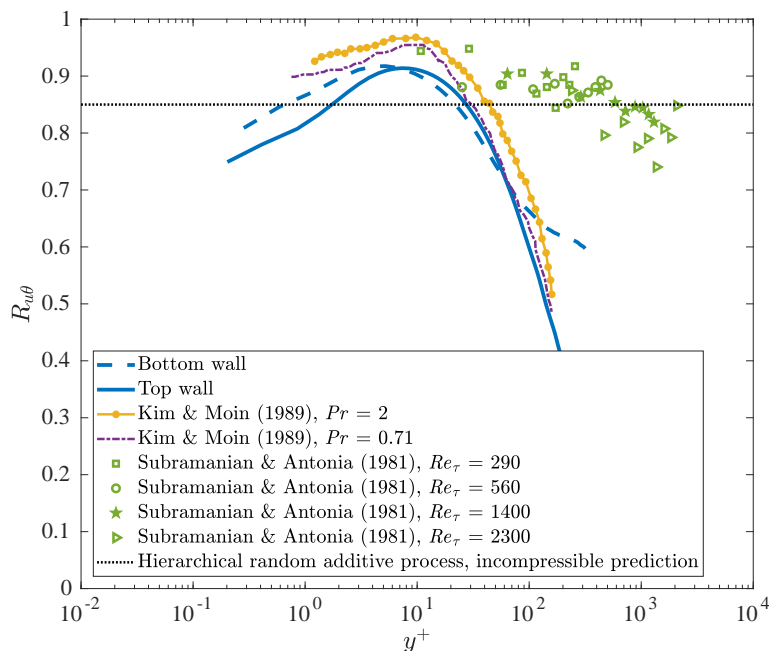


FIGURE 6. Correlation coefficient $R_{u\theta}$ versus normalized wall-normal distance y^+ for both walls as well as for various references.

coefficient does not markedly differ from previous studies that involve fluids at strictly subcritical temperatures. Very near the wall, at $y^+ \lesssim 10$, our transcritical dataset does have a lower $R_{u\theta}$ value than that of previous, subcritical DNS and experimental datasets; this is especially true for the top heated wall. This leads us to conclude that the strong variations in c_p and other associated thermal properties are responsible for a certain with nontranscritical reference cases.

5. Conclusions

The thermo-viscous structure of a channel flow at transcritical conditions is analyzed through DNS. The analysis is done with the specific focus of examining the thermal boundary layer structure, and comparison with previously reported velocity scalings. A novel, semi-local transformation is derived, following and expanding upon the work of Trettel & Larsson (2016). It is found that the canonical van Driest transformation performs well in describing the logarithmic wall layer region when compared to the semi-local scaling and transformation. Additionally, the observed scaling behavior of the streamwise energy spectrum provides support for the attached-eddy hypothesis at transcritical conditions.

Future work could involve formulation of a temperature law of the wall for describing wall-bounded flows at transcritical conditions. It is expected that this work would serve as a method for the development of accurate transcritical wall-modeled LES.

Acknowledgments

The first author gratefully acknowledges graduate funding through a Charles H. Kruger Stanford Graduate Fellowship. The authors are also grateful to Maxime Bassenne for useful and helpful discussions. The second author acknowledges funding for his participation in the 2018 CTR Summer Program.

REFERENCES

- BANUTI, D. T. 2015 Crossing the Widom-line—Supercritical pseudo-boiling. *J. Supercrit. Fluid.* **98**, 12–16.
- CHUNG, T. H., LEE, L. L. & STARLING, K. E. 1984 Applications of kinetic gas theories and multiparameter correlation for prediction of dilute gas viscosity and thermal conductivity. *Ind. Eng. Chem. Fund.* **23**, 8–13.
- CHUNG, T. H., AJLAN, M., LEE, L. L. & STARLING, K. E. 1988 Generalized multiparameter correlation for nonpolar and polar fluid transport properties. *Ind. Eng. Chem. Fund.* **27**, 671–679.
- KADER, B. 1981 Temperature and concentration profiles in fully turbulent boundary layers. *Int. J. Heat Mass Tran.* **24**, 1541–1544.
- KAWAI, S. 2016 Direct numerical simulation of transcritical turbulent boundary layers at supercritical pressures with strong real fluid effects. *AIAA Paper #2016-1934*.
- KHALIGHI, Y., HAM, F., NICHOLS, J., LELE, S. & MOIN, P. 2011 Unstructured large eddy simulation for prediction of noise issued from turbulent jets in various configurations. *AIAA Paper #2016-2886*.
- KIM, J. & MOIN, P. 1989 Transport of passive scalars in a turbulent channel flow. In *Turbulent Shear Flows 6*, pp. 85–96. Springer.
- MA, P. C., LV, Y. & IHME, M. 2017 An entropy-stable hybrid scheme for simulations of transcritical real-fluid flows. *J. Comput. Phys. Rev. Fluids* **340**, 330–357.
- MA, P. C., YANG, X. I. & IHME, M. 2018 Structure of wall-bounded flows at transcritical conditions. *Phys. Rev. Fluids* **3**, 034609.
- PATEL, A., BOERSMA, B. J. & PECNIK, R. 2017 Scalar statistics in variable property turbulent channel flows. *Phys. Rev. Fluids* **2**, 084604.
- PENG, D. Y. & ROBINSON, D. B. 1976 A new two-constant equation of state. *Ind. Eng. Chem. Fund.* **15**, 59–64.
- PIORO, I. L., KHARTABIL, H. F. & DUFFEY, R. B. 2004 Heat transfer to supercritical fluids flowing in channels — empirical correlations (survey). *Nucl. Eng. Des.* **230**, 69–91.
- PIZZARELLI, M., NASUTI, F., PACIORRI, R. & ONOFRI, M. 2009 Numerical analysis of three-dimensional flow of supercritical fluid in cooling channels. *AIAA*. **47**, 2534–2543.
- POPE, S. B. 2001 *Turbulent Flows*. Cambridge University Press.
- SCHLICHTING, H. & GERSTEN, K. 2000 *Boundary-Layer Theory*. Springer.
- SENGUPTA, U., NEMATI, H., BOERSMA, B. J. & PECNIK, R. 2017 Fully compressible low-Mach number simulations of carbon-dioxide at supercritical pressures and transcritical temperatures. *Flow Turbul. Combust.* **99**, 909–931.
- SIMEONI, G. G., BRYK, T., GORELLI, G. A., KRISCH, M., RUOCCO, G., SANTORO, M. & SCOPIGNO, T. 2010 The Widom line as the crossover between liquid-like and gas-like behaviour in supercritical fluids. *Nat. Phys.* **6**, 503–507.

- SUBRAMANIAN, C. & ANTONIA, R. 1981 Effect of Reynolds number on a slightly heated turbulent boundary layer. *Int. J. Heat Mass Tran.* **24**, 1833–1846.
- TRETTEL, A. & LARSSON, J. 2016 Mean velocity scaling for compressible wall turbulence with heat transfer. *Phys. Fluids* **28**, 026102.
- VAN DRIEST, E. R. 1951 Turbulent boundary layer in compressible fluids. *J. Atmos. Sci.* **18**, 145–160.
- YANG, X. I. & ABKAR, M. 2018 A hierarchical random additive model for passive scalars in wall-bounded flows at high Reynolds numbers. *J. Fluid Mech.* **842**, 354–380.
- YOO, J. Y. 2013 The turbulent flows of supercritical fluids with heat transfer. *Annu. Rev. Fluid Mech.* **45**, 495–525.